Phys Chem Minerals (2007) 34:201–214
DOI 10.1007/s00269-006-0139-1

ORIGINAL PAPER

On the miscibility gap in monazite–xenotime systems

P. Mogilevsky

Received: 14 September 2006 / Accepted: 19 December 2006 / Published online: 13 February 2007

Abstract The regular solid solution model has been applied to solid solubility in the monazite–xenotime systems and is verified against the available experimental data for $LaPO_4$–YPO_4 and $CePO_4$–YPO_4 systems. The model is then used to predict the miscibility gaps in a number of other monazite–xenotime systems. The implications for prospective two-phase monazite–xenotime fiber coatings for applications in ceramic matrix composites (CMCs) are discussed.

Introduction

Monazite and xenotime are common accessory minerals whose compositions and mutual solubility are important geological indicators (Heinrich 1997; Gratz 1997, 1998; Andrehs 1998; Pyle 2001; Seydoux-Guillaume 2002). These materials have also received considerable attention due to their prospective application for nuclear waste management and containment (Ewing 1995). However, it was the co-existence of alumina and monazite in natural minerals that served as a clue to the identification, development, and use of monazite ($LaPO_4$) and other materials with the ABO_4 structure as an interlayer in high temperature oxide–oxide ceramic matrix composites (CMCs) (Davis et al. 1993, 1998; Morgan et al. 1993, 1995a, b; Marshall et al. 1998; Kerans et al. 2002). Oxidation resistant fiber–matrix interlayers, capable of providing crack deflection at the fiber–matrix interface, are needed for improved toughness in ceramic composites. Today, monazite is a demonstrated oxidation resistant crack-deflecting fiber coating for oxide CMCs (Keller et al. 2003). Both monazite and xenotime are chemically stable with common structural oxides and bond weakly to them. However, xenotime has a different crystal structure and a lower coefficient of thermal expansion (CTE) than monazite, 6×10^{-6} (Hikichi et al. 1998; Subbarao et al. 1990) versus 9.6×10^{-6} (Morgan et al. 1995b), respectively. Two-phase monazite–xenotime coatings, therefore, might allow the CTE of the coating to be tailored to match the CTE of a wide range of ceramic fibers. The two-phase microstructure would also help control the undesirable grain growth in the coating. However, solid solubility between monazite and xenotime may affect both the thermal expansion and the kinetics of the grain growth in the two-phase coating. The miscibility gaps in a number of monazite–xenotime systems are evaluated based on the regular solid solution model and available experimental data.

Regular solid solution model

Let us consider a monazite–xenotime system with limited mutual solid solubility, Fig. 1.

At equilibrium between the monazite and xenotime phases, the chemical potential of both components in both phases can be written as follows:

$$\begin{cases} \mu_m^x = \mu_x^x \\ \mu_m^x = \mu_m^m \end{cases} \quad (1)$$

or

P. Mogilevsky (✉)
UES Inc., 4401 Dayton-Xenia Rd.,
Dayton, OH 45432, USA
e-mail: pavel.mogilevsky@wpafb.af.mil

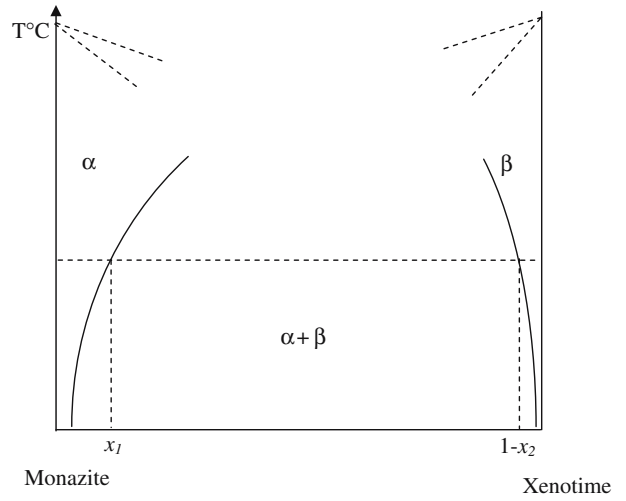

Fig. 1 Schematics of a solid section of a monazite/xenotime phase diagram with limited solubility in the solid state

$$\begin{cases} g_m^x + \mathrm{RT}\ln a_m^x = g_x^x + \mathrm{RT}\ln a_x^x \\ g_x^m + \mathrm{RT}\ln a_x^m = g_m^m + \mathrm{RT}\ln a_m^m \end{cases} \quad (2)$$

where μ, g, and a denote the chemical potential, the molar Gibbs free energy of pure components, and the activity, respectively. The lower and upper indexes represent the solvent and the solute, respectively. Thus, μ_m^x and $\mu_x{}^x$ are the chemical potentials of the xenotime component in the monazite and xenotime phases, g_m^x and $g_x{}^x$ are the molar Gibbs free energies of xenotime in a hypothetical monazite structure and in the native xenotime structure, and a_m^x and $a_x{}^x$ are the activities of xenotime in the monazite and xenotime phases, respectively.

For a regular solution, the excess enthalpy is $h^{\mathrm{ex}} = \Omega x\,(1-x)$ and the activity coefficient γ is given by:

$$\mathrm{RT}\,\ln\gamma = \Omega(1-x)^2 \quad (3)$$

where Ω is the interaction energy of the solution and x is the concentration (Gaskell 1995a). Denoting the equilibrium molar concentration of xenotime in monazite as x_1 and that of monazite in xenotime as x_2 (Fig. 1), we obtain:

$$\begin{cases} \Omega_m(1-x_1)^2 + \mathrm{RT}\ln\frac{x_1}{1-x_2} = \Delta h_x + \Omega_x x_2^2 \\ \Omega_x(1-x_2)^2 + \mathrm{RT}\ln\frac{x_2}{1-x_1} = \Delta h_m + \Omega_m x_1^2 \end{cases} \quad (4)$$

where Ω_x and Ω_m are the interaction energies of xenotime- and monazite-based solid solutions, and $\Delta h_m = h_m{}^m - h_x{}^m \approx g_m{}^m - g_x{}^m$ and $\Delta h_x = h_x{}^x - h_m{}^x \approx g_x{}^x - g_m{}^x$ are the differences in the enthalpy of formation between the monazite and xenotime (or vice versa) forms of the pure compounds, respectively.

The parameters Δh_m and Δh_x can be estimated as follows. It has been observed that the formation enthalpy of stable rare earth orthophosphates varies linearly with the rare earth ion radius (Ushakov et al. 2001). The enthalpy of formation of the dimorphic $TbPO_4$ is 286.1 ± 1.9 kJ/mol in the xenotime (stable) structure and is 283.5 ± 1.8 kJ/mol in the monazite (metastable) structure (Ushakov et al. 2001), or $\Delta h_{\mathrm{TbPO_4}} = 2.6$ kJ/mol. Assuming that the formation enthalpy of metastable monazites and xenotimes also varies linearly with the ion radius, and extrapolating to other orthophosphates, we can derive the following equations:

$$\begin{cases} \Delta h_x = \frac{R_{\mathrm{tr}} - R_x}{R_{\mathrm{tr}} - R_{\mathrm{Tb}}}\Delta h_{\mathrm{TbPO_4}} \\ \Delta h_m = \frac{R_m - R_{\mathrm{tr}}}{R_{\mathrm{tr}} - R_{\mathrm{Tb}}}\Delta h_{\mathrm{TbPO_4}} \end{cases} \quad (5)$$

where R_{tr} is the transition ion radius between the monazite and xenotime structures, at which Δh_m and Δh_x equal zero, and R_x and R_m are the ion radii of the xenotime- and monazite-forming cations, respectively. The transition from the stable xenotime to the stable monazite structure occurs between Tb and Gd (Ushakov et al. 2001). Given the ion radii of Tb and Gd, R_{Tb} = 1.04Å, R_{Gd} = 1.053 Å (Shannon 1976[1].), this correlates well with the data of Gratz and Heinrich (1998), who reported the maximum solubility of Gd in *Y*-xenotime to be 0.96, which corresponds to the mean ion radius of 1.0516 Å.

The interaction energies Ω_m and Ω_x, in turn, consist of two parts: the energy associated with transforming the solute from its stable structure to that of the solvent ($-\Delta h_x$ and $-\Delta h_m$, respectively), and the elastic energy U_{el} associated with the insertion of a substitution ion into the host lattice:

$$\Omega_{x,m} = -\Delta h_{m,x} + U_{\mathrm{el}} \quad (6)$$

The elastic energy can be expressed as follows:

$$\begin{aligned} U_{\mathrm{el}} &= 4\pi N_a E\left[\frac{R_0}{2}(R_1-R_0)^2 + \frac{1}{3}(R_1-R_0)^3\right] \\ &= 4\pi N_a \mathrm{E}R_0^3\left(\frac{y^2}{2} + \frac{y^3}{3}\right) \end{aligned} \quad (7)$$

where E is the Young's modulus of the host lattice, R_1 is the radius of the substitution ion, R_0 is the radius of the native ions of the host lattice (Brice 1975), and $y = (R_1 - R_0)/R_0$ is the fractional difference in the ion radius. If the Young's modulii of the compounds involved are known, the temperature dependence of x_1

[1] All radii cited in this study are eight coordinated ion radii

and x_2 can be obtained by solving the equations given in (4) numerically for any monazite–xenotime system.

Application to $LaPO_4$–YPO_4 and $CePO_4$–YPO_4 systems

The calculations are further simplified for the $LaPO_4$–YPO_4 and the $CePO_4$–YPO_4 systems for which the miscibility gap is strongly asymmetric and the solid solubility of monazite in xenotime is very low (Heinrich et al. 1997; Gratz and Heinrich 1997, 1998; Andrehs and Heinrich 1998; Pyle et al. 2001; Mogilevsky et al. 2006b). Neglecting the small solubility of monazite in YPO_4 ($x_2 = 0$), we obtain the following from the equations given in (4):

$$RT \ln x_1 + \Omega_m (1 - x_1)^2 = \Delta h_{YPO_4} \quad (8)$$

According to Eqs. 6 and 8, the difference in solid solubility of YPO_4 in $LaPO_4$ and in $CePO_4$ is determined by the difference in the elastic energy. Thus, if the solid solubility of YPO_4 in one of the two monazite compounds, e.g. $CePO_4$, at a given temperature is known, then the temperature at which the same level of solid solubility is reached in the other compound can be calculated:

$$R\Delta T = -\frac{\Delta U_{el}(1 - x_1)^2}{\ln x_1} \quad (9)$$

where ΔU_{el} is the difference in the elastic energy associated with the insertion of a substitution ion (Y) into the two host lattices. The room temperature Young's modulus of $LaPO_4$ monazite is $E = 133$ GPa (Morgan et al. 1995b). Although there is no available data on the Young's modulus of $CePO_4$, it must be quite close to that of $LaPO_4$[2]. Substituting the ionic radii $R_1 = R_Y = 1.019$ and $R_0 = R_{La} = 1.16$ Å or $R_0 = R_{Ce} = 1.143$ Å (Shannon 1976) into Eq. 7 produces $U_{el} = 10.7$ kJ/mol and $U_{el} = 8.2$ kJ/mol, respectively, or $\Delta U_{el} = 2.5$ kJ/mol. The temperature dependence of the YPO_4 solubility in $LaPO_4$ can now be obtained from the YPO_4 solubility in $CePO_4$ by introducing the corresponding temperature correction, as defined by Eq. 9.

The result is shown in Fig. 2, where the data on YPO_4 solubility in $CePO_4$ from 300 to 1,000°C, extrapolated to the ambient pressure of 1 atm (Gratz and Heinrich 1997) and adjusted using Eq. 9, are plotted together with the data on YPO_4 solubility in $LaPO_4$ from 1,000 to 1,600°C (Mogilevsky et al. 2006b). It is seen that both sets of data form a common trend. Equation 8 was then fitted to the combined set of data, which resulted in the best-fit parameters of $\Delta h_{YPO_4} = -8.2$ kJ/mol and Ω_m=17.4 kJ/mol. These parameters need to be compared to the values predicted by Eqs. 5–7. Substituting $R_{tr} = 1.0516$ Å (see above Discussion) and $R_Y = 1.019$ Å (Shannon 1976) into Eq. 5, we obtain $\Delta h_{YPO_4} = -7.3$ kJ/mol, which is in reasonable agreement with the best fit value of –8.2 kJ/mol. The general agreement between the best fit value of Δh_{YPO_4} and that calculated using Eq. 5 is remarkable given the relatively large uncertainties associated with R_{tr} and, especially, Δh_{TbPO_4}. Assuming that the value $\Delta h_{TbPO_4} = 2.6$ kJ/mol is the correct one, the revised value of R_{tr} that reconciles Eq. 5 with the best fit value of $\Delta h_{YPO_4} = -8.2$ kJ/mol is $R_{tr} = 1.0498$ Å, which still falls between the ion radii of Tb and Gd (1.04 and 1.053 Å, respectively). Retaining the previously chosen value $R_{tr} = 1.0516$Å, the revised value of Δh_{TbPO_4} would be –2.92 kJ/mol, which is well within the uncertainty limits associated with its experimental value (Ushakov et al. 2001). Given the value of the elastic energy for YPO_4 solution in $LaPO_4$, $U_{el} = 10.7$ kJ/mol, calculated above, the interaction energy $\Omega_m = (\Delta h_{YPO4} + U_{el}) = 18.0$ kJ/mol, in good agreement with the best fit value of $\Omega_m = 17.4$ kJ/mol.

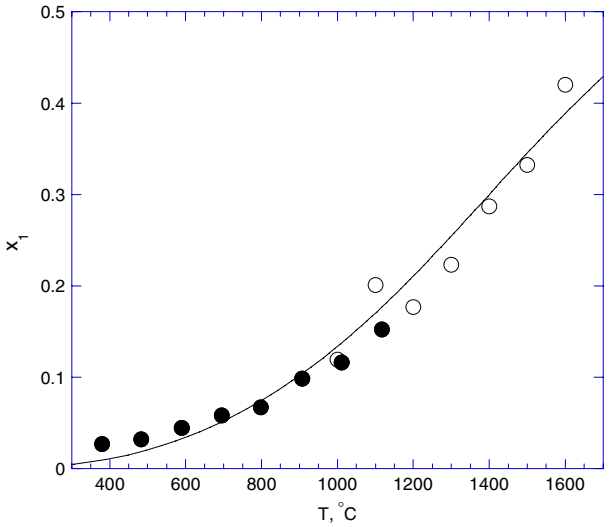

Fig. 2 Fitting of Eq. 8 to the experimental data on solid solubility of YPO_4 in $LaPO_4$ (*open symbols*, Mogilevsky et al. 2006b) combined with the data on solid solubility of YPO_4 in $CePO_4$ (Gratz and Heinrich 1997) adjusted using Eq. 9 (*filled symbols*)

[2] See Sect. 5 for more on Young's modulus of monazite and xenotime orthophosphates

Asymmetry of the miscibility gap and distribution coefficient

We can use the approach outlined above to rationalize the asymmetry of the miscibility gap in the $LaPO_4$–YPO_4 and the $CePO_4$–YPO_4 systems, where there is a much lower solubility of monazite in xenotime than vice versa (Heinrich et al. 1997; Gratz and Heinrich 1997, 1998; Andrehs and Heinrich 1998; Pyle et al. 2001; Mogilevsky et al. 2006b). Substituting Eq. 8 into the second equation given in (4) we obtain:

$$\Omega_x(1-x_2)^2+\frac{\Delta h_x-\Omega_m(1-x_1)^2}{\ln x_1}\ln\frac{x_2}{1-x_1}=\Delta h_m+\Omega_m x_1^2 \tag{10}$$

Substituting R_{La} = 1.16 Å (Shannon 1976) into Eq. 5 and again assuming R_{tr} = 1.0516 Å, we obtain Δh_m = –24.3 kJ/mol. Substituting the Young's modulus of xenotime, E = 152 GPa (Kuo and Kriven 1995; Mogilevsky et al. 2006), and the ionic radii $R_1 = R_{La}$ and $R_0 = R_Y$ into Eq. 7, we obtain U_{el} = 12.7 kJ/mol and Ω_x = 37 kJ/mol for the $LaPO_4$ solution in YPO_4 xenotime. Solving Eq. 10 numerically, we obtain the dependence of x_2 on x_1, Fig. 3a.

It is seen that when x_1 = 42% (the maximum solubility of YPO_4 in $LaPO_4$ experimentally observed at T = 1,600°C (Mogilevsky et al. 2006b)), the predicted solubility of $LaPO_4$ in YPO_4 is much smaller, x_2 = 1.7%, in agreement with the experimental results (Heinrich et al. 1997; Gratz and Heinrich 1997, 1998; Andrehs and Heinrich 1998; Pyle et al. 2001; Mogilevsky et al. 2006b). This is mainly due to the large Δh_{LaPO_4} compared to Δh_{YPO_4}, since the difference between the corresponding elastic energies is relatively small. An Arrhenius plot of the calculated Y distribution coefficient, $D_Y = x_Y^m/x_Y^x = x_1/(1-x_2)$, for the $LaPO_4$–YPO_4 and the $CePO_4$–YPO_4 systems, along with the experimental data (Heinrich et al. 1997; Gratz and Heinrich 1997), is shown in Fig. 3b. The redistribution of Y between the xenotime-based and the monazite-based solid solutions involves two concurrent reactions with activation energies of Ω_x = 37 kJ/mol and Ω_m = 18.0 kJ/mol for the $LaPO_4$–YPO_4 system and Ω_x = 30.2 kJ/mol and Ω_m = 15.4 kJ/mol for the $CePO_4$–YPO_4 system. The apparent activation energies for both systems, $E_a \approx$ 32 and $E_a \approx$ 29 kJ/mol, respectively, determined from the slopes of the Arrhenius plots, are indeed very close to the apparent activation energies expected for the process involving two concurrent reactions with activation energies of Ω_x and Ω_m. These results are in line with the established correlation between the crystal/melt partition coefficients and the elastic strain energy (Wood and Blundy 1997; Blundy and Wood 2002, 2003).

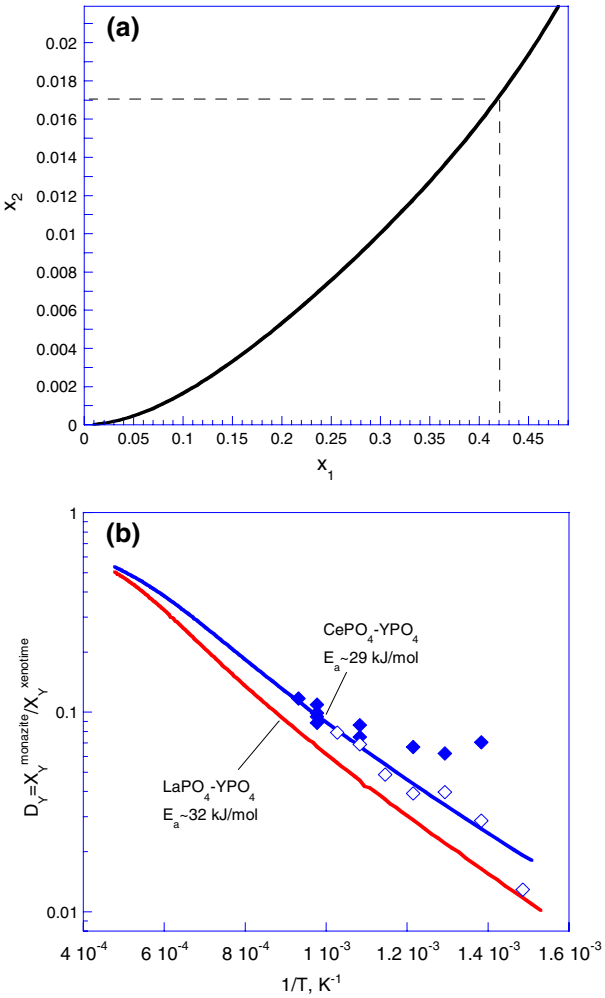

Fig. 3 **a** Calculated solubility of $LaPO_4$ in YPO_4 (x_2) as a function of the solubility of YPO_4 in $LaPO_4$ (x_1); **b** calculated Y distribution coefficient D_Y versus reciprocal temperature for $LaPO_4$–YPO_4 and $CePO_4$–YPO_4 (*solid lines*); *symbols* are experimental values (Heinrich et al. 1997; Gratz and Heinrich 1997)

Miscibility gaps in other monazite–xenotime systems

The above analysis shows that for the $LaPO_4$–YPO_4 and $CePO_4$–YPO_4 systems, Eqs. 5–7 give reasonably accurate estimates for the parameters of the equations given in (4). Therefore, miscibility gaps in other monazite–xenotime systems could be calculated in a similar manner, if the values of the Young's modulus for these compounds were available. Unfortunately, only limited data on the elastic properties of monazites and xeno-

times are available. Therefore, certain assumptions regarding the Young's modulus of other monazites and xenotimes would have to be made to calculate the miscibility gaps in these systems.

Among monazite compounds, the polycrystalline Young's modulus is only available for $LaPO_4$ (Morgan et al. 1995b), but a reasonable assumption can be made based on the well-established linear correlation between the melting temperature and the Young's modulus (Fine et al. 1984; Skinner and Zedalis 1988; Ashby 1998). The melting temperatures of La, Ce, Pr, Nd, and Sm monazites have been reported (Hikichi and Nomura 1987). A near linear correlation between the melting temperatures (Hikichi and Nomura 1987) and the rare earth ion radius has been observed (Mogilevsky et al. 2006b):

$$T_m(^\circ\mathrm{C}) = -188.96 + 1951.4R_m \tag{11}$$

where R_m is the rare-earth ion radius (Å). Thus, given the experimental Young's modulus of $LaPO_4$, E = 133 GPa (Morgan et al. 1995b), and the La ion radius, R_{La} = 1.16 Å (Shannon 1976), we obtain:

$$E_m \approx 4.8 + 110.6R_m \tag{12}$$

where E_m is in GPa and R_m is in Å.

Among xenotime compounds, the polycrystalline Young's modulus has only been measured and reported for YPO_4 (Kuo and Kriven 1995). Data on melting temperatures are equally scarce and the above method can not be used. In general, even though the packing density of the xenotime structure is lower than that of monazite, the average RE–O distances in it are smaller (Ni et al. 1995) and the structure is correspondingly stiffer. Furthermore, it has been generally established that the elastic constants of orthophosphate, orthovanadate, and orthoarsenate xenotimes decrease with the increase in the rare earth ion radius, R_x (Armbruster 1976; Mogilevsky et al. 2006a). The experimental value of the polycrystalline Young's modulus of YPO_4 (Kuo and Kriven 1995) is in good agreement with the estimate based on the elastic constants of single crystal YPO_4 (Mogilevsky et al. 2006a). Among orthophosphates with xenotime structure, full sets of elastic constants have only been reported for $LuPO_4$ (Armbruster et al. 1974) and YPO_4 (Mogilevsky et al. 2006a), leading to the self-consistent estimates of random polycrystalline Young's modulus (Berryman 2005) of E_{LuPO_4} = 202 and E_{YPO_4}= 152 GPa (Mogilevsky et al. 2006a, in good agreement with the experimental value of Kuo and Kriven (1995)). Assuming, for lack of a better alternative, a linear correlation between the Young's modulus of xenotimes and the rare earth ion radius, and given the Y and Lu ion radii, R_Y = 1.019 and R_Y = 0.977 Å (Shannon 1976), we obtain:

$$E_x \approx 1365.1 - 1190.5R_x \tag{13}$$

where E_x is in GPa and R_x is in Å. The dependence of the Young's modulus of pure xenotime and monazite compounds on the rare earth cation radius, as described by Eqs. 12 and 13, is shown in Fig. 4.

Admittedly, the linear correlations between the Young's modulus and the rare earth ion radius proposed here (Eqs. 12 and 13) are not backed up by extensive experimental evidence. It appears noteworthy, therefore, that the linear trends for monazite and xenotimes in Fig. 4 intersect at the ion radius R = 1.0455 Å, once again between the ion radii of Tb and Gd (1.04 and 1.053 Å, respectively) and close to the previously discussed estimates of R_{tr} = 1.0498 and R_{tr} = 1.0516 Å. Although far from validating Eqs. 12 and 13, it shows that they are at least consistent with the other data used here.

Solving the equations given in (4) numerically, we can obtain the temperature dependence of x_1 and x_2 for any monazite–xenotime system. Calculations were conducted for a number of monazite–YPO_4 and monazite–$LuPO_4$ systems. The choice of YPO_4 and $LuPO_4$ xenotimes was due to the fact that the Young's modulus is known for these two compounds. On the other hand, Lu is the smallest rare earth element, while Y is

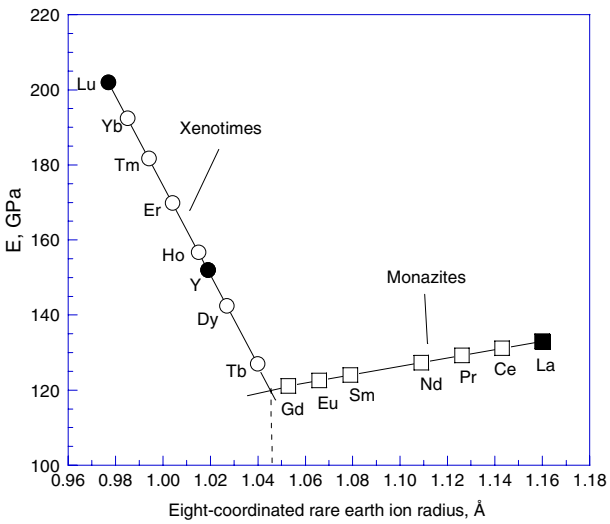

Fig. 4 Young's modulus—rare earth ion radius correlations of pure xenotime and monazite rare earth orthophosphates used in this work. *Filled symbols* are experimental values; *open symbols* are extrapolations according to Eqs. 12 and 13

one of the largest (after Dy and Tb) tri-valent elements forming xenotime orthophosphates. In addition, calculations were conducted for the $SmPO_4$–$DyPO_4$ and the $EuPO_4$–$TbPO_4$ systems. The results of these calculations are shown in Fig. 5.

In addition to the experimental data on the $CePO_4$–YPO_4 (Gratz and Heinrich 1997) and the $LaPO_4$–YPO_4 (Mogilevsky et al. 2006b) systems that were discussed earlier, limited solubility data are also available for $LaPO_4$–YPO_4, $NdPO_4$–YPO_4, $SmPO_4$–YPO_4, $NdPO_4$–$YbPO_4$ (Van Emden et al. 1996), $GdPO_4$–YPO_4 (Gratz and Heinrich 1998), and $CePO_4$–$LuPO_4$ (Lempicki et al. 1993). The available experimental data are compared to the values predicted by the present model in Table 1. There is a generally good agreement between the calculated values and the experimental ones. For the $NdPO_4$–YPO_4 system, the calculated solubility in both phases is somewhat lower than the experimental values. However, it must be noted that the experimental data on this system were obtained on samples precipitated from solution and heat treated at 1,000°C for 48 h (Van Emden et al. 1996). It has been found that at 1,000°C, longer heat treatments (100 h) were needed to equilibrate similar samples of the $LaPO_4$–YPO_4 system (Mogilevsky et al. 2006b). Accordingly, the $NdPO_4$–YPO_4 samples (Van Emden et al. 1996) might not have reached equilibrium and thus the corresponding solid solutions might have concentrations in excess of the equilibrium solubility level. Another discrepancy is for the $SmPO_4$–YPO_4 system where the calculations predict a considerably higher solubility of $SmPO_4$ in YPO_4 than the reported experimental value (0.36 vs. 0.15), even though there is a good agreement for the solubility of YPO_4 in $SmPO_4$. In the $CePO_4$–$LuPO_4$ system, 0.898% Ce for Lu substitution has been reported in Ce-doped $LuPO_4$ crystals grown from the melt at 1,360°C (Lempicki et al. 1993). The present calculations suggest that the level of Ce for Lu substitution in $LuPO_4$ at 1,360°C should be 0.93%, in good agreement with the reported experimental data.

Lastly, the very large (~96%) and virtually temperature-independent solubility of $GdPO_4$ in most xenotimes (Fig. 5a, b) should be pointed out. This is in agreement with the experimental data for $GdPO_4$–YPO_4 (Gratz and Heinrich 1998), Table 1. In addition, at least 75% solubility of $GdPO_4$ in $TbPO_4$ (Mullica et al. 1992) and in $YbPO_4$ (Mullica et al. 1990) has been reported, although the maximum solubility was not explored in those studies. In part, this has been built into the model by the choice of R_{tr} in Eq. 5, which was based on the experimental solubility of Gd in YPO_4 (Gratz and Heinrich 1998). However, since R_{tr} is only one of the model's parameters and its value is tightly bound by other experimental observations as well (see Sects. 3, 10), this agreement with the exper-

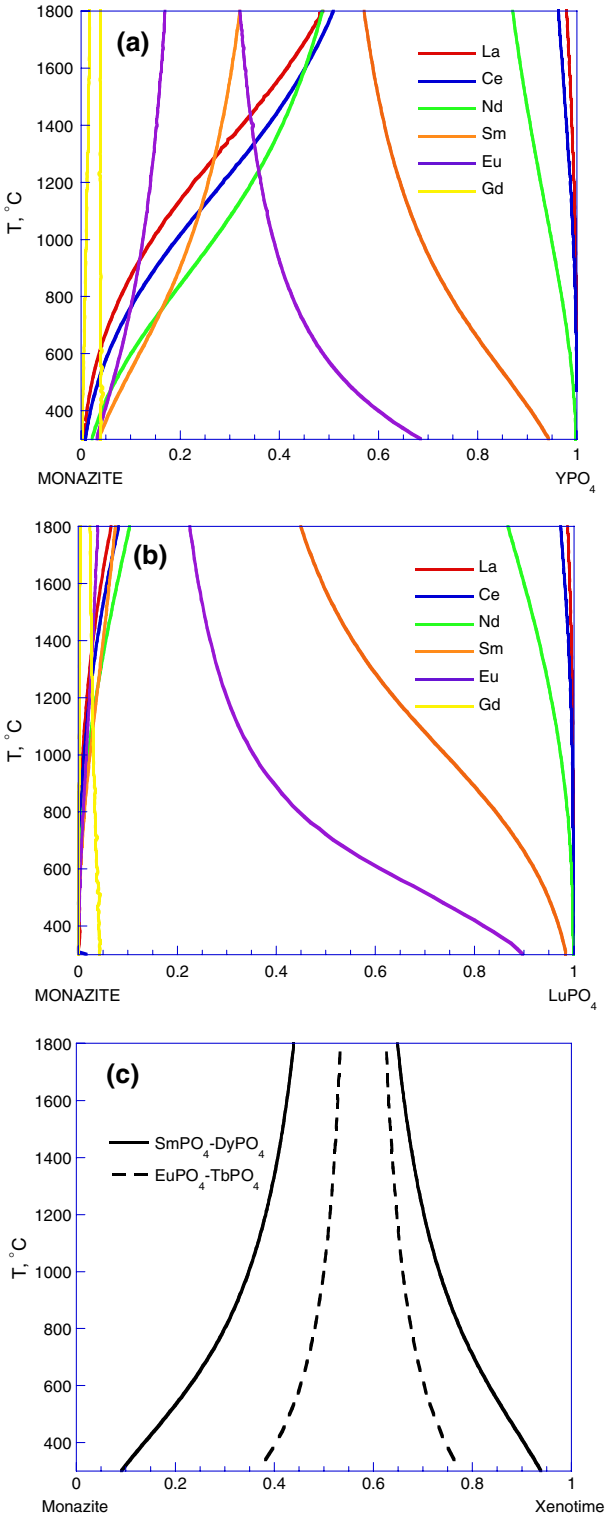

Fig. 5 Calculated miscibility gaps for a number of monazite–xenotime systems: **a** monazite–YPO_4; **b** monazite–$LuPO_4$; **c** $SmPO_4$–$DyPO_4$ and $EuPO_4$–$TbPO_4$ systems

Table 1 Comparison of calculated and experimental solubility of xenotime in monazite (x_1) and monazite in xenotime (x_2)

System	T°C	Calculated (this work)		Experimental		
		x_1	x_2	x_1	x_2	Ref.
$LaPO_4$–YPO_4	1,200	0.23	6×10^{-3}	~0.23	Less than few %	Van Emden et al. (1996)
	1,500	0.37	0.012	~0.38		
	1,590	0.41	0.014	>0.4		
$NdPO_4$–YPO_4	1,000	0.27	0.05	0.3-0.4	0.1–0.15	
$SmPO_4$–YPO_4	1,200	0.26	0.36	~0.25	~0.15	
$NdPO_4$–$YbPO_4$	1,200	0.05	0.05	<0.12	~0.06	
$CePO_4$–YPO_4	300	0.01	2.4×10^{-5}	0.03	7×10^{-3}	Gratz and Heinrich (1997)
	400	0.02	1.1×10^{-4}	0.04	8×10^{-3}	
	500	0.03	3.6×10^{-4}	0.05	7×10^{-3}	
	600	0.06	8.8×10^{-4}	0.06	7×10^{-3}	
	700	0.08	1.8×10^{-3}	0.07	0.03	
	800	0.11	3.1×10^{-3}	0.11	0.015	
	900	0.15	4.5×10^{-3}	0.13	9×10^{-3}	
	1000	0.19	7.4×10^{-3}	0.17	0.012	
$GdPO_4$–YPO_4	500–1,000	$(4–10) \times 10^{-3}$	0.96	–	0.96	Gratz and Heinrich (1998)
$CePO_4$–$LuPO_4$	1,360	3.48×10^{-2}	9.27×10^{-3}	–	8.98×10^{-3}	Lempicki et al. (1993)

imental results appears to be a significant additional validation of the model.

Implications for two-phase monazite–xenotime fiber coatings for CMCs

As mentioned in the Introduction, solid solubility between monazite and xenotime may affect both the thermal expansion and the kinetics of the grain growth in the two-phase coating. The temperature-dependent solid solubility will lead to temperature-induced variations in phase volume fractions, as well as (though less significant) changes in molar volumes, Young's modulus, and intrinsic CTE of the constituent phases (solid solutions), all of which affect the CTE of the material (Mogilevsky et al. 2006b). These effects will be particularly severe for systems with considerable asymmetry of the miscibility gap, such as $LaPO_4$–YPO_4 and $CePO_4$–YPO_4, Fig. 5a. In these systems, the CTE of the two-phase monazite–xenotime coating will increase with temperature because of the decrease of the volume fraction of the low CTE phase (xenotime), and this change is estimated to be comparable to the temperature dependence of the CTE of pure monazite (Mogilevsky et al. 2006b). In systems with low solubility in monazite but high solubility in xenotime, such as $EuPO_4$–YPO_4, $EuPO_4$–$LuPO_4$, and $SmPO_4$–$LuPO_4$ (Fig. 5a, b), the volume fraction of the low CTE phase (xenotime) will increase with temperature, and the CTE will tend to decrease, possibly offsetting the intrinsic temperature dependence of the CTE of the constituent phases. The very limited mutual solid solubility between $LaPO_4$ and $LuPO_4$ (the largest monazite-forming light rare earth element (LREE) and the smallest xenotime-forming heavy rare earth elements (HREE)), Fig. 5b, will lead to a weak temperature dependence for the phase composition and volume fractions, and the associated change in CTE will be minimal for this system. Systems with a large mutual solid solubility but a nearly symmetrical miscibility gap, such as $SmPO_4$–YPO_4 (Fig. 5a), and $SmPO_4$–$DyPO_4$ and $EuPO_4$–$TbPO_4$ (Fig. 5c) should also have relatively small CTE variations, because the phase volume fractions will be nearly independent of temperature. Among these, the $EuPO_4$–$TbPO_4$ system also has the extra benefit of having nearly the lowest Young's modulus (Fig. 4) and possibly the lowest hardness among the monazite/xenotime-based compositions, which may make it a better fiber coating for CMCs (Kerans et al. 2002). However, the disadvantage of compositions with large mutual solubility is that very little, if any, grain growth inhibition may be expected in these two-phase materials as compared to the single-phase materials.

The very large (~96%), virtually temperature-independent solubility of $GdPO_4$ in most xenotimes was pointed out in the previous section. These results mean that only 4 at.% of HREE elements or Y are sufficient to completely transform $GdPO_4$ into the xenotime structure, and even smaller amounts (<1 at. of *Y* or <0.1 at.% of Lu at 1,000°C) would shift the equilibrium into the two-phase (monazite + xenotime) region. This, as well as the slow transformation kinetics, may be partially responsible for the observation of both monazite and xenotime modifications in nominally pure $GdPO_4$ (Gratz and Heinrich 1998; Ushakov et al. 2001; Celebi and Kolis 2002). Such large solubility in

xenotimes makes $GdPO_4$ an unlikely candidate for the design of two-phase monazite/xenotime materials. However, it could be used to soften (achieve the lowest modulus, Fig. 4, and possibly hardness) stable xenotime compounds, such as YPO_4.

The choice of a particular monazite/xenotime coating system for CMCs will depend on the priorities set for the particular application, such as CTE and its temperature dependence, grain growth inhibition, or mechanical properties (elastic modulus and/or hardness). The present results can assist in choosing the optimal coating system depending on the application and design priorities.

Solid solubility in monazite/monazite and xenotime/xenotime systems

Solid solubility in monazite/monazite and xenotime/xenotime systems can be obtained from the equations given in (4). In this case, both phases have the same structure and the interaction energy of the solid solution is dominated by the elastic energy. Given the rather weak dependence of the Young's modulus of monazite on the rare earth ion radius (Fig. 4) and the nearly symmetric nature of Eq. 7, we can assume that the interaction energy (Ω) of monazite/monazite solid solutions is independent of concentration over the entire composition range, as is the case for regular solid solution. In this case, $x_1 = x_2$ and the equations given in (4) converge into the usual equation describing phase separation in regular solid solutions:

$$T_{ps} = \frac{2T_c(1-2x)}{\ln(1/x-1)} \tag{14}$$

where T_{ps} is the temperature of phase separation and $T_c = \Omega/2R$ is the critical temperature above which the solid solution is stable over the entire range of compositions (Gaskell 1995b). For xenotime/xenotime systems, the Young's modulus depends strongly on the rare earth ion radius (Fig. 4), and consequently, the elastic energy must depend on composition. Strictly speaking, in this case, the symmetrical regular solution model and the equations given in (4) do not apply. However, the limiting case of the solution behavior can be readily obtained if the interaction energy is assumed to be independent of the composition, but is set to its highest possible value for the given system.

Figure 6 shows the elastic energy of $LaPO_4$-based monazite and $LuPO_4$-based xenotime solid solutions calculated using Eq. 7 as a function of the fractional difference in the rare earth ion radius. All data fall on a common parabolic curve. Even for solid solutions consisting of the end members of both series, $LaPO_4$–$GdPO_4$ and $LuPO_4$–$TbPO_4$, the fractional difference in the rare earth ion radius is below 0.1 (Fig. 6), indicating the likelihood of complete solid solubility. The system with the highest elastic energy is $LaPO_4$–$GdPO_4$ with U_{el} ~6.3 kJ/mol, which corresponds to a critical temperature of T_c ~ 104°C. This means that in practice, all xenotime/xenotime and monazite/monazite systems should indeed exhibit the complete range of solid solution. This is in agreement with the data on $CePO_4$–$GdPO_4$ systems (Gratz and Heinrich 1998; Vance et al. 2000). Among xenotimes, at least 90% solubility in the $LuPO_4$–$TbPO_4$ system has been reported (Mullica et al. 1992).

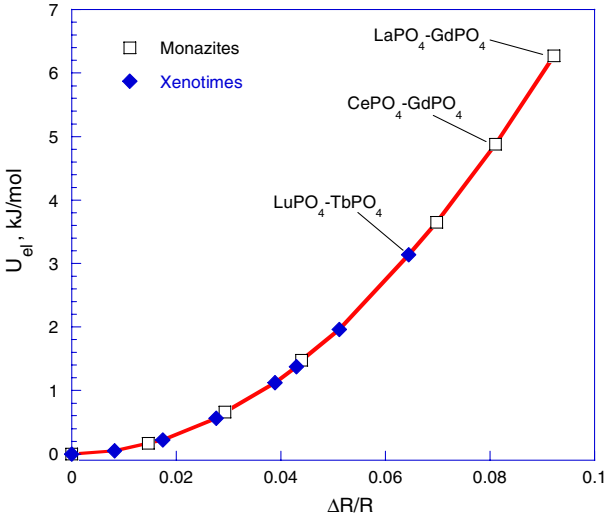

Fig. 6 Elastic energy of $LaPO_4$-based monazite and $LuPO_4$-based xenotime solid solutions

Pressure dependence of the miscibility gap

Pressure dependence of the miscibility gap, which is particularly important for geological applications (Heinrich et al. 1997; Gratz and Heinrich 1997, 1998; Andrehs and Heinrich 1998; Pyle et al. 2001; Seydoux-Guillaume et al. 2002), can be evaluated in the following manner. The monazite structure has a higher packing density (lower molar volume) than the xenotime structure (Aldred 1984; Ni et al. 1995). The cell volume of the dimorphic $TbPO_4$ is 275.9 $Å^3$ in the monazite (metastable) structure and 292.7 $Å^3$ in the xenotime (stable) structure (Ushakov et al. 2001). For $GdPO_4$ the corresponding values are 280.32 $Å^3$ in the monazite structure and 296.98 $Å^3$ in the xenotime structure (Gratz and Heinrich 1998). Therefore,

external pressure will increase the relative stability of the monazite structure and decrease the stability of the xenotime structure. As a zero approximation of the pressure dependence of the thermodynamic stability of each structure, the elastic energy of hydrostatic compression should be added to Δh_x and subtracted from Δh_m in the equations given in Eq. 4:

$$\begin{cases} \Delta h'_x = \Delta h_x + \frac{P^2}{2K_x} V_x \\ \Delta h'_m = \Delta h_m - \frac{P^2}{2K_m} V_m \end{cases} \quad (15)$$

where K_x and K_m are the bulk modulus and V_x and V_m are the molar volumes of the xenotime and monazite phases, respectively.

The excess elastic energy associated with the insertion of a substitution ion into the host lattice is also pressure dependent. External pressure should increase the excess elastic energy associated with the insertion of a larger substitution ion into the host lattice (solid solution of monazite in xenotime) and decrease it for a smaller substitution element (solid solution of xenotime in monazite). Considering this, along with the effect of hydrostatic compression on the relative stability of monazite and xenotime structures (Eq. 15), hydrostatic compression should increase the solubility of xenotime in monazite and decrease the solubility of monazite in xenotime, shifting the miscibility gap towards the xenotime side of the phase diagram.

Again as a zero approximation, we can assess the effect of external pressure on the excess elastic energy associated with ion substitution through its effect on the effective ion radius of the host lattice, R_0 in Eq. 7. Both monazite and xenotime structures consist of rigid PO_4 tetrahedra and eight- or nine-coordinated oxygen-bonded rare earth ions (Ni et al. 1995). The energy of the P–O bonds is considerably higher than that of the rare earth–O bonds (Mogilevsky et al. 2006), and the mean P–O distances remain nearly unchanged for all rare-earth orthophosphates from La to Lu (Ni et al. 1995). Furthermore, although there appears to be no high pressure structural data for either xenotime or monazite orthophosphates, PO_4 tetrahedra in aluminum, boron, and lead orthophosphates are rigid and undergo little structural change with pressure (Haines et al. 2003; Angel et al. 2001). Therefore, for this analysis, it can be assumed that, at least at room temperature, the PO_4 tetrahedra in both monazite and xenotime structures are incompressible, and under hydrostatic pressure, the compression of the lattice results from the contraction of the rare earth–oxygen bonds, which can be interpreted as a decrease of the effective radius of the rare earth ion.

The cube root of the cell volume of both monazite and xenotime orthophosphates depend linearly on the rare earth ion radius (Aldred 1984):

$$V^{1/3} = a + bR \quad (16)$$

where V is the cell volume, R is the rare earth ion radius, and a and b are constants whose values for rare earth orthophosphates with monazite and xenotime structures are given in Table 2.

For relatively low pressures ($P << K$), $V = V_0(1–P/K)$, where K is the bulk modulus, and P is the pressure. Substituting this into Eq. 16 and taking $(1– P/K)^{1/3} \approx (1 – P/3K)$, we obtain:

$$R'_0 \approx R_0 - (R_0 + a/b)\frac{P}{3K} \quad (17)$$

where R_0 is the standard effective ion radius of the host lattice at ambient pressure.

Substituting Eq. 17 into Eq. 7, we can obtain the dependence of U_{el} on the external hydrostatic pressure for any monazite–xenotime system. The results for the $LaPO_4$–YPO_4 and the $CePO_4$–YPO_4 systems are shown in Fig. 7. The bulk modulii of $LaPO_4$ and $CePO_4$ monazites (K_m=E_m/3(1-2ν) ≈ 98 GPa (Morgan et al. 1995b)) and YPO_4 xenotime (K_x=132 GPa (Mogilevsky et al. 2006a)) were assumed for these calculations.

Substituting the pressure-dependent parameters Δh_x, Δh_m, and U_{el} into the equations given in (4), we can calculate miscibility gaps in monazite–xenotime systems as a function of temperature and pressure. Figure 8 compares the results of such calculations to the available experimental data for the $CePO_4$–YPO_4 system at 800°C (Gratz and Heinrich 1997). Although in the experimentally studied pressure range of 2–15 kbar the model predicts a slightly accelerating nonlinear pressure dependence of solubility as compared to the linear empirical correlation (Gratz and Heinrich 1997, the dashed line in Fig. 8), the overall agreement between the calculated and experimental values is good. However, at higher pressures, the model predicts a much faster increase of the solubility with pressure as compared to the extrapolation of the empirical linear correlation (see inset in Fig. 8).

Table 2 Parameters a and b of Eq. (16) for rare earth orthophosphates with monazite and xenotime structures

Structure	a, Å	b
Monazite	4.6155	1.8240
Xenotime	4.4478	2.1054

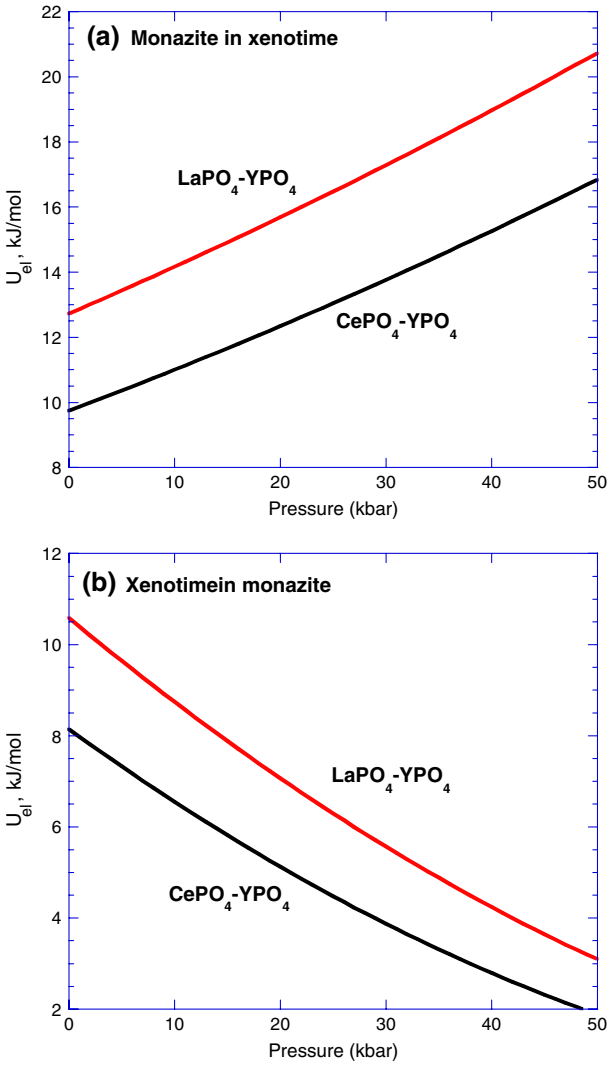

Fig. 7 Pressure dependence of the elastic energy U_{el} of **a** monazite in xenotime and **b** xenotime in monazite solid solutions for $LaPO_4$–YPO_4 and $CePO_4$–YPO_4 systems

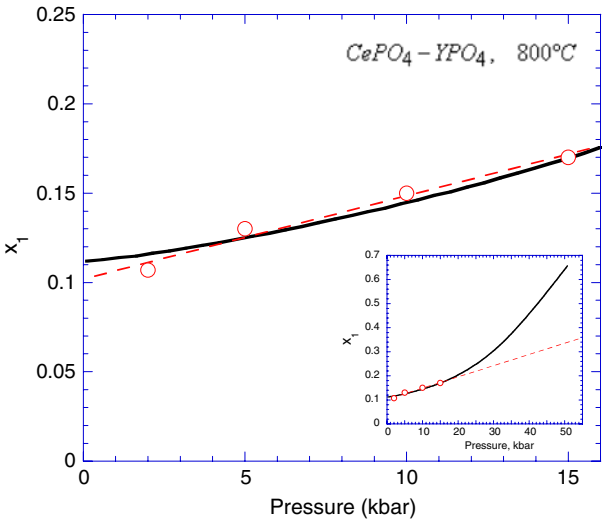

Fig. 8 Calculated (*solid line*) and experimental (*symbols*, Gratz and Heinrich 1997) pressure dependence of solubility of YPO_4 in $CePO_4$. The *dashed line* is the linear correlation (Gratz and Heinrich 1997)

The increase of xenotime solubility with pressure indicates that the excess volume of solution, $V^{ex} = \partial\Omega_m/\partial P$, is negative. The excess volume can be calculated based on the Eqs. 6, 7, 15, and 17 and at ambient pressure is –1.64 and –1.9 cm^3 for the solution of YPO_4 in $CePO_4$ and in $LaPO_4$, respectively. Given the molar volumes of YPO_4, $CePO_4$, and $LaPO_4$ (42.96, 45.26, and 46.17 cm^3, respectively (Aldred 1984)), the volumetric deviation from the ideal behavior is ~1% in both cases. This roughly corresponds to the maximum deviation from Vegard's law for the lattice parameters of ~0.3% (at 0.5 concentration). Since most measurements are for more dilute solutions, the deviation from Vegard's law becomes even less apparent. Accordingly, linear dependence of lattice parameters on composition is commonly observed for monazite and xenotime solid solutions (Gratz and Heinrich 1997, 1998; Andrehs and Heinrich 1998; Mogilevsky et al. 2006b) and these solid solutions are sometimes described as ideal (see Kolitsch and Holtstam 2004 for a review of studies on solid solutions in $REEXO_4$ systems). It should be noted, however, that at least in one study (Van Emden et al. 1996), a considerable positive V^{ex} was reported for the $NdPO_4$–YPO_4 system. However, as was pointed out in Sect. 5, the data for this system might have been collected from solution-precipitated specimens that had not reached equilibrium and thus contained Y in excess of the equilibrium solubility level.

Application to multicomponent systems

The agreement with the available experimental data demonstrates that the approach presented above is applicable to binary monazite–xenotime systems. This may be sufficient for the prospective applications in CMCs. However, the systems of interest in geological research are multicomponent. Rigorous treatment of a multicomponent system would require solving large systems of equations with multiple interaction parameters. A simplified treatment of multicomponent systems can be achieved with the present approach, provided some a-priori information is available on the distribution coefficients of the components involved.

Let us consider, as an example, the synthetic multicomponent system described by Andrehs and Heinrich (1998), whose composition was chosen to match a natural sedimentary rock (metapelite) sample (Heinrich et al. 1997). Elemental analysis of the monazite

and xenotime phases indicated that monazite-forming light rare earth elements (LREE) from La to Sm were predominantly incorporated into the monazite phase, while xenotime-forming heavy rare earth elements (HREE), as well as *Y* and Gd, were predominantly incorporated into the xenotime phase. The mean ion radii of LREE and HREE (plus *Y* and Gd) in the monazite phase were nearly independent of temperature [4] and equal to $\bar{R}_m = 1.1352 \pm 0.0002$ Å and $\bar{R}_x = 1.0193 \pm 0.0004$ Å (the uncertainties are the standard deviations based on 10 original composition measurements, (Andrehs and Heinrich 1998)). Figure 9 shows the comparison between the solid solubility calculated using the equations given in (4) for a hypothetical pseudo-binary LREE monazite/HREE xenotime system having the effective ionic radii $\bar{R}_m$ and $\bar{R}_x$ and the experimental data (Heinrich et al. 1997; Andrehs and Heinrich 1998) expressed as the mole fraction of HREE in monazite and the mole fraction of LREE in xenotime. It is seen that the model captures the experimental trend for HREE solubility in monazite fairly well. The solubility of LREE in xenotime is underestimated by a factor of 2–3.

Partitioning of trace elements between monazite and xenotime

Partitioning of trace elements between monazite and xenotime is an important geological indicator (Gratz and Heinrich 1998; Andrehs and Heinrich 1998; Seydoux-Guillaume et al. 2002; Wood and Blundy 1997; Blundy and Wood 2002, 2003). The partition (distribution) coefficient of a trace element *i* between monazite and xenotime ($D_i = x^m{}_i/x^x{}_i$) can be expressed in the form:

$$D_i = \exp\left[\frac{\Omega_x - \Omega_m}{RT}\right] \tag{18}$$

where Ω_m and Ω_x are the interaction energies of the solid solution of the trace element in the monazite and xenotime phases, respectively. These can be calculated as a function of temperature and pressure, as described above, for any trace element and any monazite–xenotime pair. Figure 10 shows a comparison of the calculated distribution coefficients and the experimental values from Andrehs and Heinrich (1998). As in the previous section, the calculations were conducted using the mean ion radius of monazite as $\bar{R}_m = 1.135$ Å and that of xenotime as $\bar{R}_x = 1.019$ Å. It should be noted that the calculated distribution coefficients depend strongly on the parameters R_{tr} and Δh_{TbPO_4} in Eq. 5. For that reason, the calculated values of the partition coefficients were best-fit to the experimental data using R_{tr} as a fitting parameter (Δh_{TbPO_4} was fixed at –2.6 kJ/mol). This resulted in the best-fit value of R_{tr} = 1.04836 Å, once again between the ion radii of Tb and Gd and very close to the values of R_{tr} = 1.0498 and R_{tr} = 1.0455 Å that were evaluated in Sects. 3 and 5, respectively.

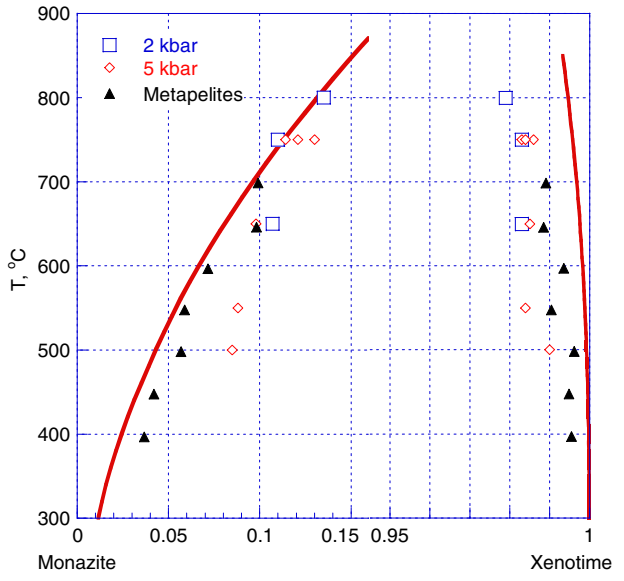

Fig. 9 Solid solubility (mole fraction of HREE in monazite and mole fraction of LREE in xenotime) in a multicomponent system. *Symbols* are experimental data (Heinrich et al. 1997; Andrehs and Heinrich 1998), solid lines are equations given in (4)

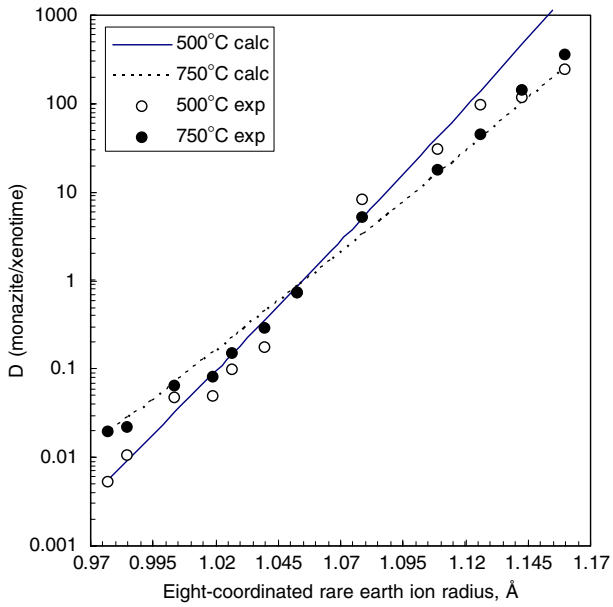

Fig. 10 Calculated (Eq. 18) and experimental (Andrehs and Heinrich 1998) distribution coefficients of rare earth elements plus *Y* between monazite and xenotime versus REE ion radius

The temperature dependence of the calculated distribution coefficients of Gd, Nd, and Y is shown in Fig. 11a along with the experimental data (Heinrich et al. 1997; Gratz and Heinrich 1997; Andrehs and Heinrich 1998). Note that while the agreement with the experimental values is very good for Gd and Nd, there is a systematic difference for *Y*. This is due to the fact that the experimental data for *Y* were obtained on systems where *Y* was a major component and not a trace element (Heinrich et al. 1997; Gratz and Heinrich 1997; Andrehs and Heinrich 1998). In this case, Eq. 18 does not apply and the data agree much better with the equations given in (4) (dashed line in Fig. 11a). The distribution coefficient decreases with temperature for monazite-forming elements (La–Eu), increases for xenotime-forming elements (Tb–Lu plus *Y*), and is virtually temperature independent for Gd. Because of its relative temperature insensitivity, the partition coefficient of Gd may not be a suitable indicator for geothermometry (Wood and Fraser 1978). D_{Nd}, on the other hand, varies by a factor of ~3 from 450 to 800°C, and D_Y varies by a factor of ~7 from 300 to 850°C. It should be noted, however, that both the present results and the experimental data (Andrehs and Heinrich 1998) on the temperature dependence of D_{Gd} are in disagreement with other data (Heinrich et al. 1997; Gratz and Heinrich 1998), where a substantial temperature dependence of D_{Gd} has been reported between 450 and 1,000°C. There is no clear explanation for this difference (Andrehs and Heinrich 1998). It seems unlikely, however, that it is related to the incorporation of U, Th, and Si in the xenotime phase in natural samples (Andrehs and Heinrich 1998), because similar results were obtained for synthetic $CePO_4$–YPO_4–$GdPO_4$ samples that presumably contained no U, Th, or Si (Gratz and Heinrich 1998).

The pressure dependence of the distribution coefficient, relative to its value at normal pressure, for a number of rare earth elements is shown in Fig. 11b. The distribution coefficients of smaller elements (HREE) are somewhat more pressure-sensitive, but compared to the difference in the absolute values, the difference in the pressure dependence of the distribution coefficient is relatively small. In all cases, the distribution coefficient increases by about 15–40% between 0 and 15 kbar. As a pressure indicator, therefore, Gd has the advantage of providing temperature independent measurements (Wood and Fraser 1978). Also, because its partition coefficient is close to 1, its value is better assessed than for La and Ce, and Yb and Lu, which have very low concentrations in either xenotime or monazite, respectively (Andrehs and Heinrich 1998).

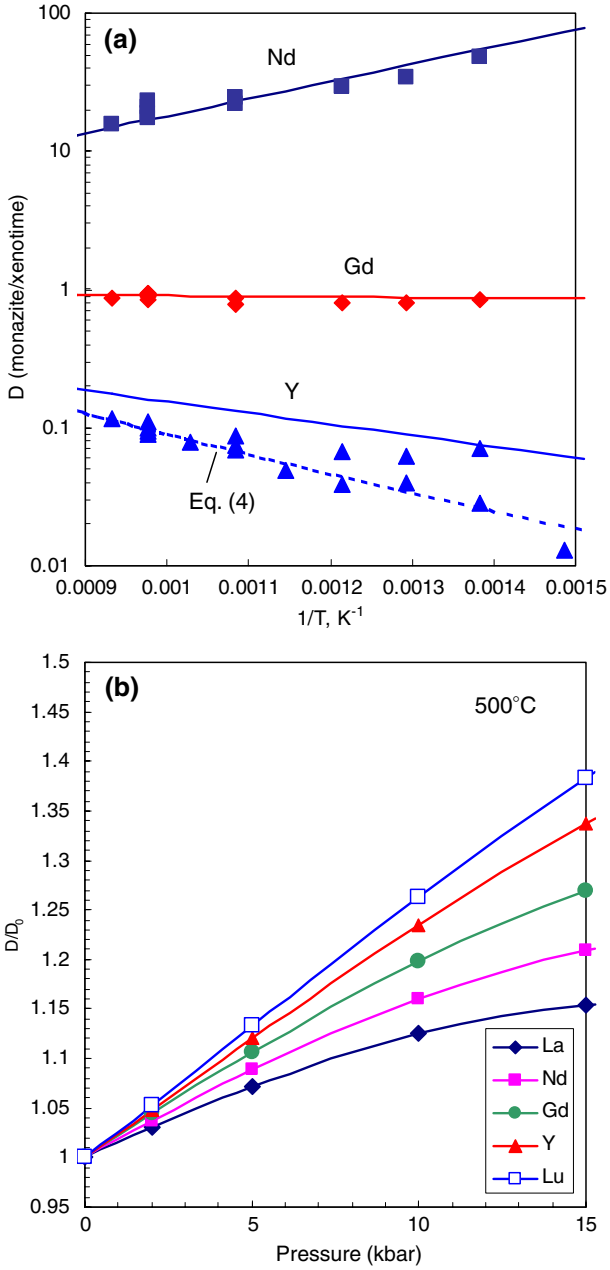

Fig. 11 **a** Temperature dependence of D_{Nd}, D_{Gd}, and D_Y. *Solid lines* correspond to Eq. 18, *symbols* are experimental values (Heinrich et al. 1997; Gratz and Heinrich 1997; Andrehs and Heinrich 1998). Dashed line is D_Y calculated according to the equations given in (4); **b** Calculated pressure dependence of the distribution coefficients of La, Nd, Gd, Y, and Lu according to the present model

Conclusions

A regular solution model has been applied to solid solubility in monazite–xenotime systems and its pressure dependence. The parameters of the model were chosen based on the available thermodynamic data and elastic properties of pure compounds. Where no

experimental data were available, linear dependence of the thermodynamic and elastic properties of monazites and xenotimes on the rare earth ion radius was assumed. The model has been verified by comparison with the available experimental data on solid solubility in a number of monazite–xenotime systems.

Good agreement between the model and the available experimental results suggests that the model could be used to predict the solubility in other monazite–xenotime systems, as well as its pressure dependence. The degree of mutual solid solubility and the asymmetry of the miscibility gaps depend on the difference in the ion radii in the usual way, but also on how close the particular ions are to the ''transition point'' between the monazite and xenotime structures. Pressure generally increases the solubility of xenotime in monazite and decreases the solubility of monazite in xenotime, shifting the miscibility gap towards the xenotime side of the phase diagram.

The model indicated complete solid solubility in all xenotime/xenotime and monazite/monazite systems, in agreement with the available experimental data for the $CePO_4$–$GdPO_4$ system.

Acknowledgments This work was supported by the Air Force Research Laboratory (AFRL), Materials and Manufacturing Directorate, under Contract No. F33615-01-C-5214. The author would like to thank Kristen Keller (UES Inc.) and Dr. Randall Hay (Air Force Research Laboratory) for critically reading the manuscript and useful suggestions.

References

Aldred AT (1984) Cell volumes of APO_4, AVO_4, and $ANbO_4$ compounds, where A=Sc, Y, La-Lu. Acta Cryst B40:569–574

Andrehs G, Heinrich W (1998) Experimental determination of REE distributions between monazite and xenotime: potential for temperature-calibrated geochronology. Chem Geol 149:83–96

Angel RJ, Bismayer U, Marshall WG (2001) Renormalization of the phase transition in lead phosphate, $Pb_3(PO_4)_2$, by high pressure: Structure. J Phys Condensed Matter 13:5353–5364

Armbruster A (1976) Infrared reflection studies on the phosphates, arsenates, and vanadates of Lutetium and Yttrium. J Phys Chem Solids 37:321–327

Armbruster A, Thoma R, Wehrle H (1974) Measurement of the elastic constants of $LuAsO_4$ and $LuPO_4$ by Brillouin scattering and determination of Debye temperatures. Phys Stat Sol A 24:K71–K73

Ashby MF (1998) Checks and estimates for material properties I. Ranges and simple correlations. Proc R Soc Lond A 454:1301–1321

Berryman JG (2005) Bounds and self-consistent estimates for elastic constants of random polycrystals with hexagonal, trigonal, and tetragonal symmetries. J Mech Phys Sol 53:2141–2173

Blundy JD, Wood BJ (2002) Prediction of crystal-melt partition coefficients from elastic moduli. Nature 372:452–454

Blundy JD Wood BJ (2003) Partitioning of trace elements between crystals and melts. Earth Planet Sci Lett 210:383–397

Brice JC (1975) Some thermodynamic aspects of the growth of strained crystals. J Crystal Growth 28:249–253

Celebi AS, Kolis JW (2002) Hydrothermal synthesis of xenotime-type gadolinium orthophosphate. J Am Ceram Soc 85:253–254

Davis JB, Lofvander JPA, Evans AG, Bischoff E, Emiliani ML (1993) Fiber coating concepts for brittle matrix composites. J Am Ceram Soc 76:1249–1257

Davis JB, Marshall DB, Housley RM, Morgan PED (1998) Machinable ceramics containing rare-earth phosphates. J Am Ceram Soc 81:2169–2175

Ewing RC, Weber WJ, Clinard FW Jr (1995) Radiation effects in nuclear waste forms for high-level radioactive waste. Prog Nuclear Energy 29:63–127

Fine ME, Brown LD, Marcus HL (1984) Elastic constants versus melting temperature in metals. Scripta Metal 18:951–956

Gaskell DR (1995a) Introduction to metallurgical thermodynamics, 3rd edn. Taylor& Francis, Washington, p 258

Gaskell DR (1995b) Introduction to metallurgical thermodynamics, 3rd edn. Taylor & Francis, Washington, p 279

Gratz R, Heinrich W (1997) Monazite–xenotime thermobarometry: experimental calibration of the miscibility gap in the binary system $CePO_4$–YPO_4. Am Mineral 82:772–780

Gratz R, Heinrich W (1998) Monazite–xenotime thermometry. III. Experimental calibration of the partitioning of gadolinium between monazite and xenotime. Eur J Mineral 10:579–588

Haines J, Chateau C, Le′ger JM, Bogicevic C, Hull S, Klug DD, Tse JS (2003) Collapsing cristobalitelike structures in silica analogues at high pressure. Phys Rev Lett 91:015503/1-4

Hayhurst T, Shalimoff G, Edelstein N, Boatner LA, Abraham MM (1981) Optical spectra and Zeeman effect for Er^{3+} in $LuPO_4$ and $HfSiO_4$. J Chem Phys 74:5449–5452

Heinrich W, Andrehs G, Franz G (1997) Monazite–xenotime miscibility gap thermometry: I. An empirical calibration. J Metamorphic Geol 15:3–17

Hikichi Y, Ota T, Daimon K, Keiji H, Hattori T, Mizuno M (1998) Thermal, mechanical, and chemical properties of sintered xenotime-type RPO_4 (R = Y, Er, Yb, or Lu). J Am Ceram Soc 81:2216–2218

Hikichi Y Nomura T (1987) Melting temperatures of monazite and xenotime. J Am Ceram Soc 70:C252–C253

Keller KA, Mah T, Parthasarathy TA, Boakye EE, Mogilevsky P, Cinibulk MK (2003) Effectiveness of monazite coatings in oxide/oxide composites in extending life after long-term exposure at high-temperature. J Am Ceram Soc 86:325–332

Kerans RJ, Hay RS, Parthasarathy TA, Cinibulk MK (2002) Interface design for oxidation-resistant ceramic composites. J Am Ceram Soc 85:2599–2632

Kolitsch U, Holtstam D (2004) Crystal chemistry of $REEXO_4$ compounds (X = P, As, V). II. Review of $REEXO_4$ compounds and their stability fields. Eur. J Mineral 16:117–126

Kuo DH, Kriven WM (1995) Characterization of yttrium phosphate and yttrium phosphate/yttrium aluminate laminate. J Am Ceram Soc 78:3121–3124

Lempicki A, Berman E, Wojtowicz AJ, Balcerzyk M, Boatner LA (1993) Cerium-doped orthophosphates: new promising scintillators. IEEE Trans Nuclear Sci 40:384–387

Marshall DB, Morgan PED, Houley RM, Cheung JT (1998) High-temperature stability of the Al_2O_3–$LaPO_4$ system. J Am Ceram Soc 81:951–956

Mogilevsky P, Zaretsky EB, Parthasarathy TA, Meisenkothen F (2006a) Composition, lattice parameters, and room temper-

ature elastic constants of natural single crystal xenotime from Novo Horizonte. Phys Chem Minerals 33:691–698
Mogilevsky P, Boakye EE, Hay RS (2006b) Solid solubility and thermal expansion in $LaPO_4$–YPO_4 system. J Am Ceram Soc (submitted)
Morgan PED, Marshall DB (1993) Functional interfaces for oxide/oxide composites. Mat Sci Eng A162:15–25
Morgan PED, Marshall DB (1995b) Ceramic composites of monazite and alumina. J Am Ceram Soc 78:1553–1563
Morgan PED, Marshall DB, Housley RM (1995a) High temperature stability of monazite–alumina composites. Mat Sci Eng A195:215–222
Mullica DF, Sappenfield EL, Boatner LA (1990) A structural investigation of several mixed lanthanide orthophosphates. Inorg Chim Acta 174:155–159
Mullica DF, Sappenfield EL, Boatner LA (1992) Single-crystal analysis of mixed ($Ln/TbPO_4$) orthophosphates. J Solid State Chem 99:313–318
Ni Y, Hughes JM, Mariano AN (1995) Crystal chemistry of the monazite and xenotime structures. Am Mineral 80:21–26
Pyle JM, Spear FS, Rudnick RL, McDonough WFM (2001) Monazite–xenotime-garnet equilibrium in metapelites and a new monazite-garnet thermometer. J Petrol 42:2083–2107
Seydoux-Guillaume A-M, Wirth R, Heinrich W, Montel JM (2002) Experimental determination of the Th partitioning between monazite and xenotime using analytical electron microscopy and X-ray diffraction Rietveld analysis. Eur J Mineral 14:869–878
Shannon RD (1976) Revised effective ionic radii and systematic studies of interatomic distance in halides and chalcogenides. Acta Crystallogr A32:751–767
Skinner DJ, Zedalis M (1988) Elastic modulus versus melting temperature in aluminum based intermetallics. Scripta Metal 22:1783–1785
Subbarao EC, Agrawal DK, McKinstry HA, Sallese CW, Roy R (1990) Thermal expansion of compounds of zircon structure. J Am Ceram Soc 73:1246–1252
Ushakov SV, Helean KB, Navrotsky A, Boatner LA (2001) Thermochemistry of rare-earth orthophosphates. J Mater Res 16:2623–2633
Van Emden B, Thornber MR, Graham J, Lincoln FJ (1996) Solid solution behaviour of synthetic monazite and xenotime from structure refinement of powder data. In: Advances in X-ray Analysis—the proceedings of the Denver X-ray Conferences, pp 2-15 (available on-line at http://www.icdd.com/resources/axa/vol40/V40_404.pdf)
Vance ER, Carter ML, Begg BD, Day RA, Leung SHF (2000) Solid solubilities of Pu, U, Hf, and Gd in candidate ceramic phases for actinide waste immobilization. Materials research society symposium–proceedings, vol 608, pp 431–436
Wood BJ, Blundy JD (1997) A predictive model for rare earth element partitioning between clinopyroxene and anhydrous silicate melt. Contrib Mineral Petrol 129:166–181
Wood BJ, Fraser DG (1978) Elementary thermodynamics for geologists. Oxford University Press, Oxford, pp 128–134